Tribology International 183 (2023) 108371

Contents lists available at ScienceDirect

Tribology International

journal homepage: www.elsevier.com/locate/triboint

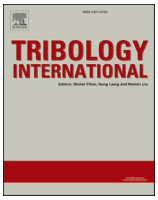

One-step laser ablation synthesis of magnetic nanoparticles with carbon coating for tribological applications

Valentina Piotto [a], Lucio Litti [a], Valentina Zin [b,*], Moreno Meneghetti [a,*]

[a] Department of Chemical Sciences, University of Padova, via Marzolo 1, Padova 35131, Italy
[b] Institute of Condensed Matter Chemistry and Technologies for Energy, National Research Council of Italy, C.so Stati Uniti 4, 35127 Padova, Italy

ARTICLE INFO

Keywords:
Magnetic nanoparticles
Laser ablation
Carbon
Multi-functional materials
Wear
Nanolubricant

ABSTRACT

Among different materials able to reduce wear and friction in tribological couplings, there are lubricant nanofluids obtained by dispersing suitable nanoparticles into a host fluid. Carbon-based nanomaterials are known to be effective additives, but their efficiency can be further improved by combination with magnetic compounds. Unfortunately, the preparation of such bifunctional materials often require complex syntheses or need post-synthesis functionalization processes, thus increasing costs and reducing reliability. Herein, a simple and cost-effective one-step synthesis method, based on laser ablation in solution, is used to produce magnetic responsive nanoparticles surrounded by a carbon matrix to be exploited as lubricating additives. The lubricating colloidal solutions are thus easily obtained without the use of surfactants nor multi-step processes, which can contaminate the final product or increase production costs. They exhibit a very good stability and reduce the wear coefficient of almost 50% in presence of an applied magnetic field in respect to the base fluid alone. The importance of the presence of the carbon matrix surrounding the magnetic core to develop a positive tribological behaviour has been proved.

1. Introduction

Nanofluids are engineered fluids containing nanosized additives, as metals, ceramics, nitrides, carbon nanostructures, which enhance the properties of a base fluid, i.e. water, ethylene glycol, propylene glycol, thermal oil, and confer it new functional properties such as thermal conductivity [1,2], optical [3,4], magnetic [5] and tribological properties [6,7]. In magnetic nanofluids, the dispersed additives are constituted by magnetic nanoparticles [8,9], and the colloidal suspensions show tunable magnetic and fluid properties which can be controlled by the application of an external magnetic field [10,11]. A wide range of carrier fluids is available and some magnetic nanofluids are commercially offered to satisfy different applications, for example in heat transfer systems [12].

Ferrites, mostly used for producing soft or hard magnets for domestic or industrial applications, are among materials suitable to modify the properties of a host fluid. They have generated an increasing interest in modifying both metals [13], ceramics [14], polymers [15,16] and fluids properties [17], thus obtaining composites and nanofluids with enhanced properties. Ferrites are metal-oxide ceramics made of a mixture of Fe_2O_3 and either small proportions of one or more additional metallic elements. These materials provide several benefits and cannot be easily replaced by other materials, as they are inexpensive, chemically stable, no toxic and environmental friendly and have enhanced magnetic, electric and thermal properties [18–20]. Ferrite nanoparticles are part of a large group of magnetic nanoparticles (MNPs), and have recently gained a considerable attention in various application fields, ranging from biomedical to industrial. The properties of ferrites are affected by several factors, including the synthesis technology, the chemical composition, the microstructure and the distribution of cations in the tetrahedral and octahedral sites into the lattice. Outstanding properties of ferrites, like mechanical strength, high hardness and wear resistance [21], make them very versatile. In combination with other properties such as dimensional stability and temperature and corrosion-resistance, ferrites are promising also for wear resistance applications. Among them, strontium ferrite ($SrFe_{12}O_{19}$) is a M-type hexaferrite ($SrO{:}6Fe_2O_3$) having higher saturation magnetization, coercivity and Curie temperature. So far, strontium ferrite has been used for high-density magnetic recording media and microwave devices [22], due to its large magnetocrystalline anisotropy [23]. It represents a good candidate for tribological applications [24], considering its chemical inertness and outstanding corrosion resistance, thanks to which it does

* Corresponding authors.
E-mail addresses: valentina.zin@cnr.it (V. Zin), moreno.meneghetti@unipd.it (M. Meneghetti).

https://doi.org/10.1016/j.triboint.2023.108371
Received 19 December 2022; Received in revised form 13 February 2023; Accepted 25 February 2023
Available online 7 March 2023

not take part in tribo-oxidative processes and does not undergo degradation due to wear phenomena. These peculiarities represent the reason why this material has been selected for the synthesis of nanoparticles by laser ablation and the subsequent preparation of nanofluids with anti-wear properties. Limiting wear means minimizing material loss, the degradation of sliding surfaces and the extension of functionality. The friction reduction and anti-wear mechanisms of lubricating nano-additives are generally acknowledged as tribofilm formation, mending or polishing effect during friction processes [25,26].

The application of a magnetic field adds a further degree of freedom to control the behaviour of magnetic nanoparticles and of the related nanofluids [27]. Among various additives, the magnetic nanoparticles dispersed in lubricating liquids (magnetic fluid) are attracting great attention due to several advantages over other nanoparticles [28,29]. The recovery of nanoparticles after use together with the enhancement of their overall safety, recyclability and sustainability are critical issues that need to be overcome. The specific behaviour under applied magnetic field is affected by the concentration, shape and size of the dispersed nanoparticles, as well as on the magnetic field features themselves [6]. One major challenge to the proper functioning of additives dispersed in lubricants is the difficult penetration of nanofluid into the friction pair due to the close contact at the interface, for instance during cutting of difficult-to-process materials such as titanium alloys [30]. To improve the efficiency of NPs transport from nanofluids and therefore the working efficiency, magnetic field-assisted technology was introduced into the machining process to achieve changes in cutting mode. Zhang et al. [31] and Guo et al. [32] applied an external magnetic field to the contact area between the tool and the workpiece and investigated the action of a Fe_3O_4 containing nanofluid with different magnetic field parameters, obtaining encouraging results. Despite several studies about nanoparticles in the tribological field, the stability of the nanodispersions against sedimentation is still a critical point, since nanoparticles tend to agglomerate with each other. Therefore, dispersants need to be used to increase the stability time of nanoparticles into host fluids. Good results can be obtained modifying the nanoparticles' surface by reacting with a surfactant, thus obtaining nanoparticles that are coated or functionalized [33]. For this purpose, the laser ablation synthesis in solution (LASiS) method has been taken into consideration in this work, to create stable and long-lasting suspensions.

To authors' knowledge, no in-depth studies of the tribological properties of nanoferrite containing fluids are available in the literature. In this work, both friction and wear behaviours of nanoferrite-modified fluids have been investigated, under the action of an external applied magnetic field. Multiphase nanoparticles for tribological applications are usually obtained via multi-step syntheses, where an inorganic core is usually coated with organic molecules or carbon-based materials to confer multi-properties and/or enhanced stability, thus avoiding aggregation and sedimentation, when used as dispersed additives in a fluid. The control of these nanomaterials is commonly achieved with chemical bottom-up approaches and post-synthesis treatments at high pressure or temperature, and/or in a controlled atmosphere [34]. In the last two decades a top-down synthesis technique like LASiS [35], has become interesting due to its green approach that allows the syntheses of different types of nanoparticles in a wide range of solvents [36]. This technique exploits the high local temperature and pressure generated by a pulsed laser beam focused on a bulk material immersed in a liquid. The ablation of the target material generates nanoparticles that are directly dispersed in the liquid phase, creating a stable colloidal dispersion. The produced nanoparticles do not require any stabilizing agent, like surfactants or capping molecules, because of their native surface charge.

In this work, the laser ablation methodology has been exploited as a one-step synthesis technique to easily produce bifunctional magnetic responsive nanoparticles to be dispersed into a host fluid for tribological applications. The tribological behaviour of produced suspensions has been evaluated also in presence of a variably oriented magnetic field in order to investigate the possibility of driving the anti-wear action of the dispersed nanoparticles.

2. Materials and methods

2.1. Nanofluid preparation

Strontium ferrite nanoparticles coated with a carbon matrix were obtained via LASiS. A strontium ferrite ($SrFe_{12}O_{19}$) target purchased from *Supermagnete* (FE-S-05–05) was placed at the bottom of a vial and covered with 2 cm of toluene (*Sigma Aldrich*). A nanosecond pulsed laser beam (doubled Nd:YAG laser at 532 nm, 6 ns, 20 Hz) was focused on the surface of the target and the fluence was adjusted to 2 J/cm^2. During the ablation, the target was moved to avoid formation of craters that negatively affect the laser fluence. A purification step was applied to the colloidal solution, consisting of three complete attractions of the colloidal solution with magnets (*Supermagnete*, S-10–20-N) and redispersion in 2 mL of EtOH the first two times and in 2 mL of HCl (0.05 M) the third time. The last step was used to dissolve hydroxides present in solution. Then the magnetic nanoparticles were collected by magnetic attraction applying a magnet (*Supermagnete*, S-5–25-N) for 30 min and then dispersed in bidistilled water with an ultrasonic bath. Nanoparticles without the carbon coating were obtained by laser ablation of the same target in bidistilled water. In this case, only the acid treatment was used to dissolve hydroxides. The obtained nanoparticles will be referred as T-SFIO (Toluene – Strontium Ferrite Iron Oxide) for the laser-ablated nanoparticles in toluene and A-SFIO (Aqueous – Strontium Ferrite Iron Oxide) for those ablated in water. Nanofluids were prepared in order to contain 0.1%$_{wt}$ nanoadditives.

2.2. Nanofluid characterization

Extinction spectra were recorded with a Cary 5000 spectrometer (*Agilent Technologies)*. UV–vis extinction spectroscopy was used to get indirect information on size, size distribution, state of aggregation, and NP concentration. A FEI TECNAI G2 transmission electron microscope (TEM) was used for morphological characterization, whereas hydrodynamic diameter and surface potential of the nanoparticles were evaluated by DLS and ζ-Potential (*Malvern instrument Zetasizer Nano* operating at 633 nm and 173°). XRD measurements were performed with a *Philips X'Pert* goniometer working in Bragg-Brentano geometry and recorded using a graphite monochromator. Elemental analysis was obtained with a *Zeiss Sigma HD SEM* microscope equipped with Schottky FEG source and an EDX from *Oxford Instruments* (x-act PentaFET Precision). Raman scattering was recorded with a *Renishaw InVia micro-Raman* focusing a 514 nm laser on dried sample with a 50x objective. Before use, the colloidal solutions were sonicated for several minutes. A contact profiler (*Bruker*, Dektat XT) was used to analyse the substrate damaged by the movement of an alumina ball.

2.3. Wear tests and worn surface analysis

The tribological analysis was carried out at room temperature, with a Bruker UMT-2 tribotester, set for pure sliding contact geometry, equipped with a load cell up to 10 N and operating in ball-on-flat configuration. The non-conformal contact between a spherical Al_2O_3 counterbody and a Si(100) wafer substrate, was investigated, with and without the presence of a variably oriented 50 mT applied magnetic field, i.e. axial direction with respect to the sliding plane. The Al_2O_3 balls, produced according to ASTM F 2094 standard with a certified hardness of 1500 HV, were supplied by RGPBALLS S.r.l. The reason for selecting Al_2O_3 balls as counterparts was dual: on one side, aluminum oxide is remarkably harder than silicon, thus providing considerable wear on the Si surface, remaining almost unaltered. On the other side, possible contamination from counterbody would not generate confusion in the interpretation of results obtained in post-mortem characterization. The mean roughness prior to wear tests for Al_2O_3 balls was Ra=

0.005 μm, while Si wafer had mirror-like finishing. Tribological experiments lasted for 120 min and a frequency of 1 Hz was set, via linear reciprocating motion mode, developing boundary lubrication conditions. The normal load was hold constant in order to obtain 750 MPa of initial Hertzian contact pressure [37]. The picture of the equipment and the schematic representation of the setup are visible in Fig. 1(a) and (b).

Experiments were performed also in presence of an axial ring magnet placed onto the Si substrate, so that field lines crossed the contact zone and were variably oriented, i.e. entering or exiting in respect to the sliding plane. Pure water was used as reference fluid. The magnet was fixed on the substrates, while the counterbody could move inside it, progressively developing the wear track for following characterizations. A quantity equal to 5 mL of lubricating fluid was used in each trial, sufficient to completely cover the contact patch, avoiding starvation during test execution. The fluid was completely renewed for each repetition of the experiment. Each test was repeated three times to ensure repeatability and reliability of the results. The topology of wear tracks was examined by FE-SEM (Sigma, Zeiss) coupled with X-EDS spectroscopy (Oxford Instruments). On each sample, wear scars dimensions and depths were measured with a contact stylus profiler (Dektak XT, Bruker). The volumetric wear loss was also estimated according to ASTM G133–05 [38], using the geometrical relations given in the standard. A descriptive statistical approach was applied to the results of the tribological tests carried out, repeated several times to verify the reproducibility of the results obtained.

3. Results and discussion

3.1. Laser ablation synthesis

Magnetic nanoparticles used to prepare the tribological nanofluids were easily obtained by LASiS of a target of magnetic material immersed in an organic solvent. In the present case a strontium ferrite bulk target was ablated in toluene with ns pulses of a duplicated Nd:YAG laser. The synthesis protocol produced spherical magnetic nanoparticles (T-SFIO), which appeared to be surrounded by a carbon matrix phase. A sample called A-SFIO, used for comparison, was produced by LASiS of the strontium ferrite target immersed in pure water. The dimensional characterization shows that both types of nanoparticles are spherical and that A-SFIO nanoparticles have a lognormal distribution centred at 80 nm [39], whereas for T-SFIO the distribution is centred at 10 nm. The smaller dimension of T-SFIO nanoparticles can be attributed to the presence of the carbon matrix around them that limits their growth.

TEM image of T-SFIO and A-SFIO nanoparticles are reported in Fig. 2 (a-b), respectively. It can be observed that the T-SFIO nanoparticles appear embedded within a carbon matrix, while in A-SFIO no traces of any matrix surrounding nanoparticles can be detected, and nanoparticles appeared aggregated in micrometric clusters.

Extinction spectra of the colloidal solutions was characterized with a spectrophotometer in the range 200–1350 nm, as visible in Fig. 2(c). The comparison between the spectra of T-SFIO and A-SFIO samples shows a contribution below 600 nm for the T-SFIO nanoparticles, ascribable to the presence of the carbon matrix. Dynamic Light Scattering (DLS) of the T-SFIO sample shows that the nanoparticles have an average dynamical dimension of 250 nm, but a high degree of polydispersity makes this value not reliable and that is due to the variable distribution of the carbon matrix around the nanoparticles. ζ-potential analysis confirms that the nanostructures are stable in water, thanks to their native negative charge, producing a negative potential of −31 mV. Similar results have been observed for the DLS of a solution of A-SFIO [39].

Low intensity and noisy signals have been observed by XRD diffraction of T-SFIO and A-SFIO samples, because nanoparticles exhibited poor crystallinity. Therefore, the identification of the magnetic phases was not possible. For this reason, Raman analysis, with a 514 nm laser excitation, was instead preferred for the characterization of the produced samples. Following a parallel study of the A-SFIO [39], which allowed identifying the presence of magnetite and Sr-ferrite in these nanoparticles, similar Raman spectra for the T-SFIO were obtained. The presence of both phases likely originated from the fact that the ablation process was performed in air, and therefore the oxidation of iron to magnetite occurred. However, a reliable quantitative evaluation of the two phases was difficult from the collected Raman spectra. Raman spectra above 1000 cm^{-1} were exploited for the detection of the carbon matrix formed in T-SFIO, as highlighted in Fig. 3, where two intense characteristic bands of the carbon material, namely the G band at 1590 cm^{-1} and the D band at 1330 cm^{-1} can be observed. The spectrum also shows a low intensity band at 2690 cm^{-1}, which is usually associated with the 2D band characteristic of more ordered carbon phases, like graphite. These results are consistent with the optical spectrum of T-SFIO reported in Fig. 2(c) and allow concluding that the observed matrix surrounding the magnetic nanoparticles effectively corresponds to a graphitic-like phase.

A more quantitative analysis of the relative presence of Sr-ferrite and magnetite in T-SFIO and A-SFIO could be obtained from X-EDS measurements. The Fe/Sr atomic ratio was found to be (26.8 ± 1.9) for A-SFIO and (18.2 ± 4.3) for T-SFIO. Considering the presence of the two magnetic phases, Sr-ferrite can be estimated to be present, according to their formula, for 17% and 32% in A-SFIO and T-SFIO respectively. The larger presence of Sr-ferrite in the T-SFIO sample was expected because the carbon matrix, present on these nanoparticles, hinders further oxidation of Fe. Since Sr-ferrite has been proved to possess superior

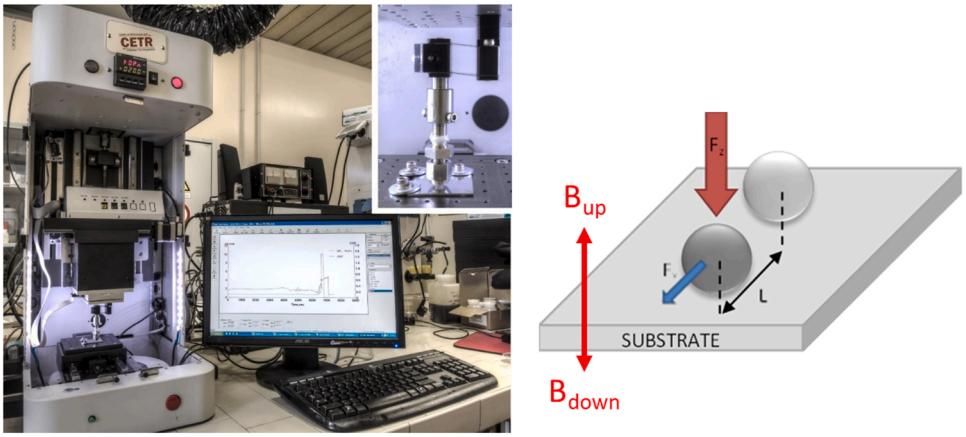

Fig. 1. (a) Picture of the equipment used and (b) scheme of the used configuration for tribological tests.

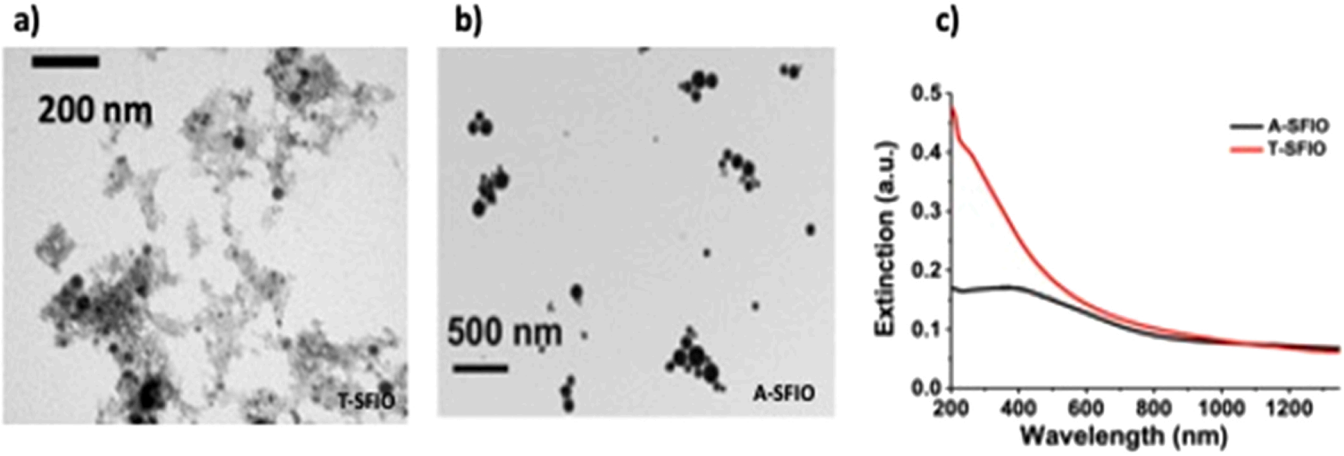

Fig. 2. a) TEM image of T-SFIO; b) TEM image of A-SFIO (from ref. 30); c) Exctinction spectra of A-SFIO (black line) and T-SFIO (red line).

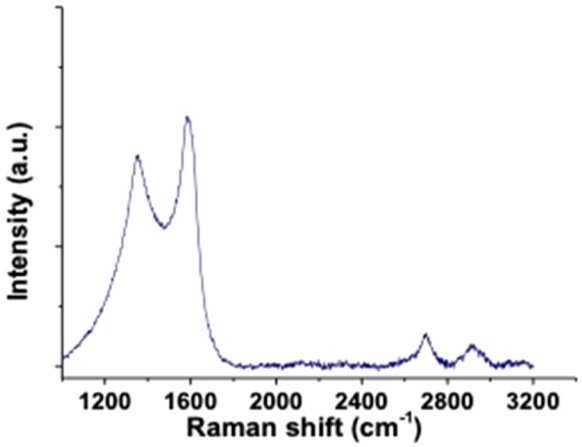

Fig. 3. Raman spectrum of the T-SFIO sample from 1100 to 3200 cm^{-1}.

tribological properties, a better behaviour was expected for T-SFIO nanofluid during wear tests.

3.2. Tribological characterization

In order to evaluate the tribological behaviour of the nanoparticles enclosed in the carbon matrix, the T-SFIO and, for comparison, A-SFIO have been tested in the same operating conditions. The variations of the friction coefficient (CoF) with sliding time for different samples and conditions had a similar general trend, i.e. the CoF remained at a relatively stable level after a short run-in time. The values of stable-state friction coefficient are reported in Table 1.

Both bare (A-SFIO) and carbon coated (T-SFIO) magnetic nanoparticles possess a minor improvement of tribological properties with respect to water, used as a reference, without the presence of a magnetic field. This probably derives from the low probability of the presence of the nanoparticles within the contact region. However, in presence of a magnetic field, which force the particles to remain in the tribological contact region, a strong difference was observed between the A-SFIO and T-SFIO. For T-SFIO, an improvement can be detected, although small, whereas a notable increase of the friction coefficient (+34%) is recorded for A-SFIO sample. The poor lubrication effect of A-SFIO can be understood considering that the magnetized nanoparticles can aggregate within the contact zone, and act as an abrasive, getting stuck in the track during the sliding process. Similar results were achieved also by Liu et al. [40], according to whom an applied magnetic field increased the CoF of magnetite-loaded nanogels. The aggregation of the T-SFIO nanoparticles is, on the other hand, contrasted by the carbon matrix, which also behaves as a local lubricant. Wear scar profiles (see below) gave more evidence to these results.

Table 1
Friction coefficients of A-SFIO and T-SFIO without and in presence of a magnetic field and, for comparison, the friction coefficient of water.

Sample	CoF	Sample	CoF
H_2O	0.23 ± 0.02		
A-SFIO	0.22 ± 0.03	T-SFIO	0.22 ± 0.03
A-SFIO B_{UP}	0.31 ± 0.06	T-SFIO B_{UP}	0.22 ± 0.04
A-SFIO B_{DOWN}	0.30 ± 0.01	T-SFIO B_{DOWN}	0.21 ± 0.03

The Archard's wear model [41] was used herein to evaluate the anti-wear properties of lubricious nanofluids, since it generally correlates the wear volume with the hardness of the softest sliding body, the applied normal load and the total sliding distance, according to the following formula (Eq. 1):

$$K = \frac{\Delta V \bullet H}{F_N \bullet s} \quad (1)$$

where K is the dimensionless generalized wear coefficient, and it is therefore a measure of the severity of wear, ΔV is the worn volume (m^3), s is the sliding distance (m), F_N is the normal contact force (N), and H is the hardness (Pa) of the surface material that is worn away. Geometrical features of wear scars, obtained with A-SFIO and T-SFIO, also in presence of a magnetic field, are compared in Fig. 4, also considering the behaviour of pure water.

In Fig. 4, one observes that T-SFIO can effectively preserve the Si surface from wear phenomena and surface damage in presence of the magnetic field. On the contrary, A-SFIO nanoparticles, in presence of the applied magnetic field, behave as wear accelerating agent. These data confirm the above results for the CoF. In absence of the magnetic field, both nanofluids perform similarly to pure water. The behaviour of the A-SFIO nanoparticles agrees with the observations of several authors, who found that in the absence of a magnetic field the wear scar profiles of a magnetic nanofluid is very similar to its base fluid. Instead, in its presence numerous particles enter the contact area and abrasive wear occurs due to their aggregation in linear chains, forced by the action of the magnetic field [42–44]. The different behaviour of the T-SFIO nanoparticles can be understood, as above, for the presence of the surrounding carbon matrix.

Numerical results are reported in Table 2. For A-SFIO nanoparticles in the presence of the magnetic field, an increase of 2.6 times of the wear coefficient with respect to the reference fluid is observed, whereas for T-SFIO, a decrease of 1.8 times of the wear coefficient was found in the

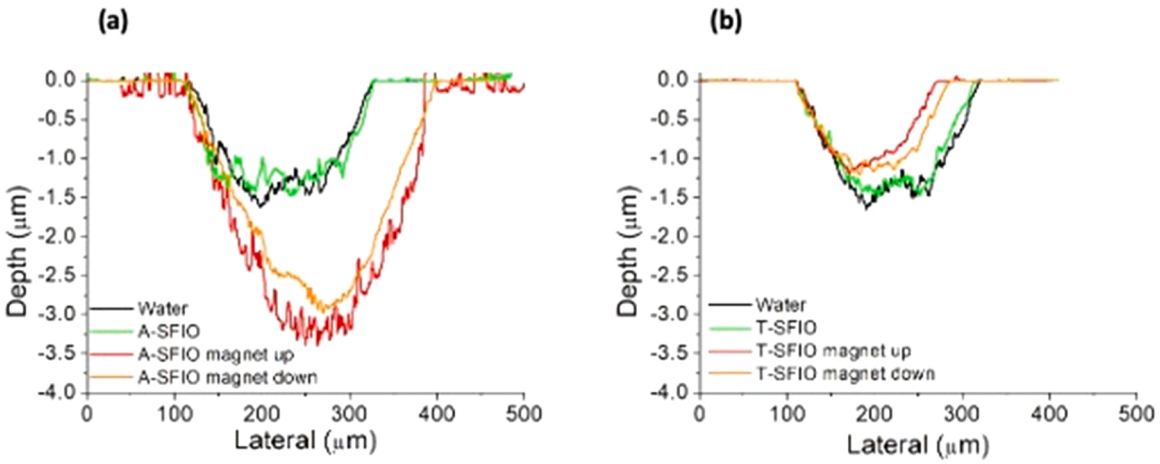

Fig. 4. Comparison of wear scars profiles on Si surfaces treated with (a) A-SFIO and (b) T-SFIO nanofluids.

Table 2
Characterization of the wear scars comparing track depths, worn volumes and wear coefficients.

Sample	Magnetic field	Track depth Z (μm)	Worn volume V (μm^3)	Wear coefficient K
Water	NO	1.62 ± 0.03	834267	$1.99 \cdot 10^{-4}$
T-SFIO	NO	1.51 ± 0.02	794267	$1.9 \cdot 10^{-4}$
T-SFIO	YES (up)	1.18 ± 0.04	454800	$1.09 \cdot 10^{-4}$
T-SFIO	YES (down)	1.20 ± 0.01	538800	$1.29 \cdot 10^{-4}$
A-SFIO	NO	1.47 ± 0.03	848587	$2.0 \cdot 10^{-4}$
A-SFIO	YES (up)	3.16 ± 0.22	2183333	$5.21 \cdot 10^{-4}$
A-SFIO	YES (down)	2.91 ± 0.07	1938000	$4.63 \cdot 10^{-4}$

same operating conditions. The poor lubricating activity of A-SFIO nanoparticles arises from the abrasive action of the aggregates acting as a third body within the contact area, thus interacting antagonistically at the tribological contacts and abrasively removing material from the coupled surfaces [45]. Since the maximum intensity of the applied magnetic field is located at the centre of the developing wear scar, it keeps the nanoparticles concentrated in that region for the entire duration of the test, thus intensifying their effect. In Fig. 5, SEM images of the wear scar regions on Si substrates with pure water and magnetic nanofluids are shown. The magnetic field, with the maximum intensity located at the centre of the developing wear scar, concentrates the magnetic nanoparticles in that region, keeping them in position for the entire duration of the test and, therefore, intensifying their effect.

In all cases, the tribological coupling appear to work in severe wear mode and the wear regime is assumed to be surface-initiated fatigue, generating cracks and micropitting [46–48]. Generally, in contact fatigue, plastic deformation layers and cracks form as the local stress overcomes the elastic limit of the contact materials. Sliding concurs to the initiation and propagation of cracks, which mostly initiate from the surface. This phenomenon is generated by repeated over-rolling and consequently by cyclic contact stresses acting on the sliding surfaces. Due to the elastic deformation, material removal can be caused by fatigue phenomena: the process starts after a relatively low deformation at contacts between abrasive particles and the substrate. Thus, in abrasive wear, one of the mechanisms of material removal is related surface

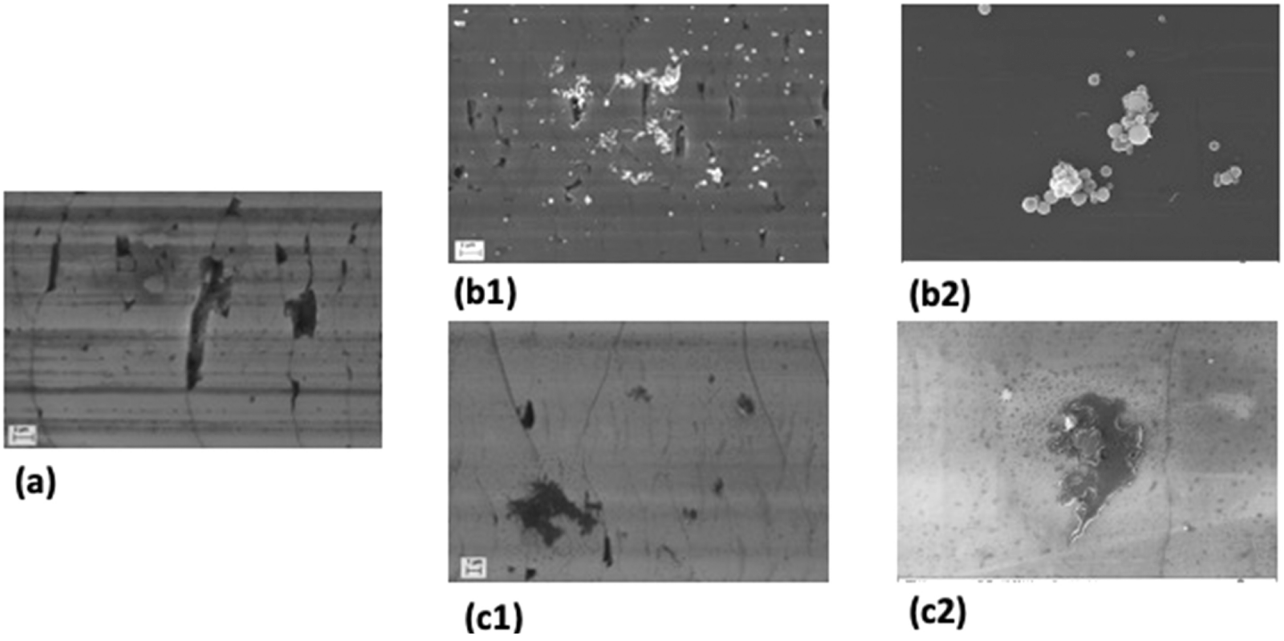

Fig. 5. SEM images of the wear tracks for the tests conducted with (a) pure water; (b1) A-SFIO in presence of a magnetic field (configuration 'up'); (b2) magnification of (b1); (c1) T-SFIO in presence of a magnetic field (configuration 'up'), (c2) magnification of (c1).

fatigue wear [49]. In Fig. 5(a) and (b1), it clearly appears that surface cracks are responsible of wear damage of the sliding surfaces, where also numerous signs of micropitting can be detected. This phenomenon is detrimental for the good functioning of devices, gears and sliding surfaces, because it involves premature failure. Comparing Fig. 5(a) and (c1), it can be noticed that, although some superficial cracks are still present, the number of pits is significantly reduced for the tests with T-SFIO.

Differently from A-SFIO sample, T-SFIO nanoparticles exhibit an improved tribological behaviour, owing to their carbon coating, which favours the lubricating action and protects the underlying silicon surface from fatigue and micropitting. Moreover, the carbon shell not only provides an available lubricious phase that decreases friction phenomena, but also prevents the further aggregation of magnetic nanoparticles, as observed in the other case. The synergistic effect between carbon shell and magnetic nanoparticles has been already observed and described [50]. In absence of the magnetic field, it is likely that the nanoparticles are expelled from the sliding area by the movement of the counterbody and hence they can no longer operate within the tribological pair. Therefore, the same beneficial behaviour cannot be observed without the application of the magnetic field. According to some interpretations of the friction mechanism [51,52], it can be assumed that during the sliding process the T-SFIO nanoparticles buffer to avoid the direct contact between the silicon substrate and the counterpart. At the same time, the lubricating carbon phase also fills the surface gap and decreases the contact pressure [53,54]. The nanoadditives are continuously supplied, as T-SFIO nanoparticles are progressively deformed or invalidated within the sliding contact zone, thanks to the action of the applied magnetic field, resulting in a self-lubrication effect. This is confirmed by the observation that several aggregates of A-SFIO nanoparticles, visible in Fig. 5(b1) and 4(b2), are stuck in the track, even after the final washing treatment, whereas the T-SFIO nanoparticles are almost absent, as visible in Fig. 5(c1) and 4(c2). Further confirmation is obtained by X-EDS measurements inside the tracks in the last case, which evidenced only the presence of carbon and neither iron nor strontium, demonstrating that magnetic nanoparticles did not deposit at the tribological interface. The surface of all the counter bodies were also investigated, to confirm that there was no wear on the Al_2O_3 balls. Only a few light scratches were found on the spheres, and the loss of material was not detected even with a precision balance. No traces of Al were found inside the wear traces, analysed via X-EDS. Consequently, the transfer of material from the alumina balls could be excluded.

Final roughness at the bottom of the wear scar is also a useful index of the benefits derived by the use of the lubricating nanofluid. The roughness was measured by stylus profilometry after the tribological tests. The results are reported in Fig. 6 and Table 3.

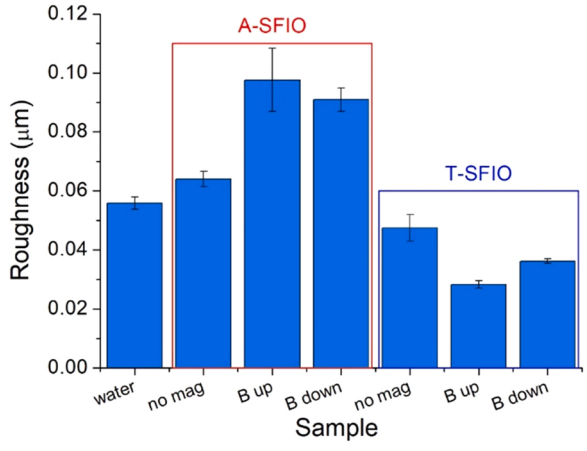

Fig. 6. Roughness Ra measured at the bottom of the wear scars after tribological tests.

Table 3
Roughness (Ra) mean values for each measured wear scar.

Sample	R_a (μm)	Var
H_2O	0.056 ± 0.002	-
A-SFIO	0.064 ± 0.003	+ 14.3%
A-SFIO B_{UP}	0.098 ± 0.011	+ 75.0%
A-SFIO B_{DOWN}	0.091 ± 0.004	+ 62.5%
T-SFIO	0.047 ± 0.004	-16.1%
T-SFIO B_{UP}	0.028 ± 0.001	-50.0%
T-SFIO B_{DOWN}	0.036 ± 0.001	-35.7%

A-SFIO nanoparticles, forming quite large aggregates, act as abrasive third body, increasing the wear phenomena, and inducing a greater mean surface roughness, with a maximum enhancement of 75%. Conversely, T-SFIO nanoparticles exhibit a beneficial decrease of the final surface roughness with a maximum reduction of 50%, thus confirming the above considerations about the protective action of the carbon shell when the magnetic field is applied and the lubricious phase is therefore confined within the contact area.

4. Conclusions

A simple and cost-effective one-step laser ablation synthesis of a Sr-ferrite target in toluene, at ambient conditions, was exploited to produce magnetic responsive nanoparticles surrounded by a lubricious carbon matrix to be used as additives into a host fluid for anti-wear purposes. The magnetic core was found to be composed by Sr-ferrite and magnetite. The magnetic properties of the nanoparticles were exploited to confine them within the contact area of a tribological coupling by the application of a magnetic field also thus avoiding the leakage of the nanofluid from the contact area and its pollution in the environment. The carbon matrix surrounding the magnetic core conferred to the nanoparticles interesting anti-wear properties, which could be observed especially in the wear coefficient and in the final roughness of the produced wear scars. Halving of the wear coefficient and 50% reduction of the worn surface roughness prove that the carbon coated nanoparticles, produced in toluene, are promising additives for tribological applications. Therefore, the LASiS methodology endorses to be a simple approach for easily producing nanoparticles and the selection of appropriate synthetic conditions (laser pulses, target materials, solvents) opens new possibilities for obtaining nanostructures with multifaceted properties.

Statement of originality

I declare that this article is our original work and it is submitted for first publication to Tribology International. The article has not been published and is not being submitted or considered for publication elsewhere. The text, illustrations, or any other materials included in the article contains no violation of any existing copyright and does not infringe any rights of third parties. All authors participated in the work in a substantive way are prepared to take public responsibility for the work.

Funding

This research did not receive any specific grant from funding agencies in the public, commercial, or not-for-profit sectors.

Declaration of Competing Interest

The authors declare that they have no known competing financial interests or personal relationships that could have appeared to influence the work reported in this paper.

Data Availability

No data was used for the research described in the article.

References

[1] Ajeeb W, Murshed SMS. Therm Sci Eng Prog 2022;30:101276.
[2] Lenin R, Joy PA, Bera C. J Mol Liq 2021;338:116929.
[3] Wahab A, Hassan A, Qasim MA, Ali HM, Babar H, Sajid MU. J Mol Liq 2019;289:111049.
[4] Han X, Zhao X, Huang J, Qu J. Renew Energy 2022;188:573–87.
[5] Joseph SA, Mathew S. Chem Chem 2014;79:1382–420.
[6] Zin V, Agresti F, Barison S, Litti L, Fedele L, Meneghetti M, et al. Tribol Int 2018;127:341–50.
[7] Zhang Q, Song H, Wu B, Feng W, Li X, Jiao Y, et al. Wear 2021;466–467:203586.
[8] Nabeel Rashin M, Hemalatha J. Ultrasonics 2012;52:1024.
[9] Saidur R, Leong K, Mohammad H. Renew Sustain Energy Rev 2011;15:1646–68.
[10] Angayarkanni S, Philip J. Adv Colloid Interface Sci 2015;225:146–76.
[11] Patel JK, Parekh K. Ultrasonics 2015;55:26–32.
[12] Kharat Prashant B, Kounsalye Jitendra S, Shisode Mahendra V, Jadhav KM. J Supercond Nov Magn 2019;32:341–51.
[13] Maleki A, Taherizadeh AR, Issa HK, Niroumand B, Allafchian AR, Ghaei A. Ceram Int 2018;44(13):15079–85.
[14] Chu H, Jiang J, Wang F, Ju S, Wang L, Wang D. Constr Build Mater 2022;318(7):125967.
[15] Munteni C, Eni C, Graur I, Ungureanu C, Bodor M. IOP Conf Ser: Mater Sci Eng 2017;174:012025.
[16] Darwish Moustafa A, Zubar Tatiana I, Kanafyev Oleg D, Zhou Di, Trukhanova Ekaterina L, Trukhanov Sergei V, et al. Nanomaterials 2022;12:1998.
[17] Kharat Prashant B, More SD, Somvanshi Sandeep B, Jadhav KM. J Mater Sci: Mater Electron 2019;30:6564–74.
[18] Amani Mohammad, Amani Pouria, Kasaeian Alibakhsh, Mahian Omid, Wongwises Somchai. J Mol Liq 2017;230:121.
[19] Amiri Mahnaz, Akbari Ahmad, Ahmadi Meysam, Pardakhti Abbas, Salavati-Niasari Masoud. J Mol Liq 2018;249:1151.
[20] Vedrtnam A, Kalauni K, Dubey S, Kumar A. AIMS Mater Sci 2020;7:800–35.
[21] Matsumoto M, Morisako A, Takei S. J Alloy Compd 2001;326:215–20.
[22] Kimiabeigi M, Widmer JD, Long R, Gao Y, Goss J, Martin R, et al. IEEE Trans Ind Electron 2015;63:113–22.
[23] Yang QH, Zhang HW, Liu YL, Wen QW. Mater Lett 2009;63:406–8.
[24] N.R. Panchal, R.B. Jotania, in H. C. Patel et al. (eds.), Proc. Int. Conf. Adv. Tribol. Eng. Syst. (2014) 175–180.
[25] Dai W, Kheireddin B, Gao H, Liang H. Tribol Int 2016;102:88–98.
[26] Tang Z, Li S. Curr Opin Solid State Mater Sci 2014;18:119–39.
[27] Mulka R, Zajączkowski B, Neuber E, Buschmann MH. Int J Thermofluids 2022;14:100152.
[28] Trivedi K, Parekh K, Upadhyay RV. Mater Res Express 2017;4:114003.
[29] Liñeira del Río JM, López ER, González Gómez M, Yáñez Vilar S, Piñeiro Y, Rivas J, et al. Nanomaterials 2020;10:683.
[30] Zhang K, Li Z, Wang S, Wang P, Zhang Y, Guo X. J Manuf Process 2023;85:556–68.
[31] Zhang L, Guo XH, Zhang KD, Wu Yo, Huang Q. J Mater Process Tech 2020;284:116764.
[32] Guo XH, Huang Q, Wang CD, Liu T, Zhang Y, He H, et al. J Mater Process Tech 2022;299:117382.
[33] Chen Y, Renner P, Liang H. Lubricants 2019;7:7.
[34] Ghosh P, Narayan KN, Das C. JCOMC 2020;2:100018.
[35] Amendola V, Meneghetti M. J Mater Chem 2007;17:4705–10.
[36] Amendola V, Rizzi GA, Polizzi S, Meneghetti M. J Phys Chem B 2005;109:23125–8.
[37] Bushan B. Modern Tribology Handbook. Boca Raton, FL, USA: CRC Press LLC; 2001.
[38] ASTM G133-05. Standard Test Method for Linearly Reciprocating Ball-on-Flat Sliding Wear. ASTM International; 2016.
[39] Piotto V, Litti L, Omelyanchik A, Martucci A, Riello P, Peddis D, et al. J Mater Chem C 2022;10:3819–25.
[40] Liu G, Cai M, Wang X, Zhou F, Liu W. ACS Macro Lett 2016;5(1):144–8.
[41] Archard JF. J Appl Phys 1953;24:981–8.
[42] Shahrivar K, Ortiz AL, De Vicente J. Tribol Int 2014;78:125–33.
[43] Sohn JW, Choi SB, Lee ChH, Cho MW. Adv Mater Res 2009;79–82:83–6.
[44] Ku J, Chen H, He K, Yan Q. Miner Eng 2015;79:10–6.
[45] Bingley MS, Schnee S. Wear 2005;258:50–61.
[46] Lainé E, Olver AV, Beveridge TA. Tribol Int 2008;41(11):1049–55.
[47] Morales-Espejel GE, Rycerz P, Kadiric A. Wear 2018;398–399:99–115.
[48] Oila A, Bull SJ. Wear 2005;258(10):1510–24.
[49] M. Hokka, V.T. Kuokkola, P. Siitonen, J. Liimatainen, Proc. Int. Conf. Exp. Mech., Italy (2004).
[50] Huang J, Li Y, Jia X, Song H. Tribol Int 2019;129:427–35.
[51] Thampi AD, Prasanth MA, Anandu AP, Sneha E, Sasidharan B, Rani S. Mater Today Proc 2021;47:4919–24.
[52] Pawar RV, Hulwan DB, Mandale MB. J Clean Prod 2022;378:134454.
[53] Zin V, Barison S, Agresti F, Colla L, Pagura C, Fabrizio M. RSC Adv 2016;6:59477–86.
[54] Lv X, Cao L, Yang T, Wan Y, Gao J. Part Sci Technol 2020;38:568–72.